The Effect of Crystal Mismatch on the Thermoelectric Performance Enhancement of Nano Cu$_2$Se

Yunus Demirci[1], Aminu Yusuf[1], Bejan Hamawandi[2], Muhammet S. Toprak[2]* and Sedat Ballikaya[3]*

[1]Department of Electrical-Electronics Engineering, Istanbul University Cerrahpasa, Istanbul, Turkey, [2]Department of Applied Physics, KTH Royal Institute of Technology, Stockholm, Sweden, [3]Department of Physics, Istanbul University, Istanbul, Turkey

In the past decades, Cu$_{2-x}$Se compounds have attracted great attention due to the inclusion of non-toxic and abundant elements, besides having a promising thermoelectric (TE) performance. In this work, we investigated the effect of a crystal mismatch of a nanoinclusion phase on the TE properties of Cu$_{2-x}$Se. Nano-Cu$_2$Se was synthesized using microwave assisted thermolysis, while the p-type skutterudite, Fe$_{3.25}$Co$_{0.75}$Sb$_{12}$ (FeCoSb), compound was synthesized using a chemical alloying route. Nano-Cu$_2$Se, and (nano-Cu$_2$Se)$_{1-x}$(nano-FeCoSb)$_x$ composites, where $x = 0.05$ and 0.1, were prepared via mechanical alloying followed by Spark Plasma Sintering process. Structural properties were evaluated by PXRD and SEM analysis, while the high temperature transport properties were examined via electrical conductivity, Seebeck coefficient, and thermal conductivity measurements in the temperature range of 300–800 K. Powder X-ray diffraction (PXRD) confirmed a single phase of nano Cu$_2$Se, while the samples with FeCoSb inclusion consist of two phases as Cu$_2$Se and CoSb$_3$. SEM micrographs of all samples show that Cu$_2$Se has randomly oriented grains with different sizes. Cu$_2$Se samples with a FeCoSb inclusion show a rather different structure. In these samples, a rod-shaped FeCoSb phase, with a size varying between 20 and 100 nm, showed an inhomogeneous distribution in the structure and stacked between the Cu$_2$Se layers. Transport data indicate that crystal mismatch between Cu$_2$Se and FeCoSb has a strong effect on the TE transport properties. Electrical conductivity decreases but Seebeck coefficient enhances with nano FeCoSb inclusion. Total thermal conductivity was suppressed by 30% and ZT value enhanced by 15% with 5% nano FeCoSb inclusion at 750 K, likely due to a decrease in the electronic contribution of the thermal conductivity. Structural and transport data show that small amount of nanoinclusion of FeCoSb has a beneficial effect on the TE performance of nano Cu$_2$Se at temperatures below 800 K.

Keywords: thermoelectric effect, microwave assisted thermolysis, nano Cu$_2$Se, nano Fe$_{325}$Co$_{075}$Sb$_{12}$, crystal mismatch, thermal conductivity

INTRODUCTION

In an effort to reduce global warming, which results from the burning of fossil fuels, various alternative energy sources have been identified. Thermoelectric (TE) materials and devices are one of the promising alternatives and sustainable energy sources which can convert heat energy directly into electrical power. TE materials-based technologies have been incorporated into space missions and are now gaining more attention for terrestrial applications. For more than a decade, this technology has not been used in a large scale, this is because of its inherent low conversion efficiency (Bell, 2008; Snyder et al., 2008; Julian Goldsmid, 2009). This conversion efficiency is proportional to the efficiency of the TE material, which can be determined by a factor called figure of merit Z. Its dimensionless form is given as $ZT = S^2 \sigma T / \kappa$, consisting of the Seebeck coefficient (S), the electrical conductivity (σ), absolute temperature (T), and the thermal conductivity κ ($= \kappa_L + \kappa_e$), where κ_e is electronic and κ_L is the lattice contribution to thermal conductivity). A good TE material should have a high power factor ($S^2 \sigma$) and a low thermal conductivity (Bell, 2008; Snyder et al., 2008; Julian Goldsmid, 2009). In an attempt to get a higher $ZT > 2$, an extrinsic semiconductor with good electronic properties (high charge carrier mobility) is generally selected and various methods that will reduce the thermal conductivity as much as possible are being explored. Several approaches have been used to increase the efficiency of TE materials. Such approaches include the Phonon Glass Electron Crystal paradigm (Rowe, 2006; Beekman et al., 2015), the formation of bulk nano-composites (Hsu et al., 2004; Poudel et al., 2008), the use of band resonant states to enhance the density of states (Heremans et al., 2008), the composition and temperature induced band convergence (Pei et al., 2011; Liu et al., 2012), using materials with extreme inharmonicity of lattice vibrations (Morelli et al., 2008), ultra-fast solidification techniques (Li et al., 2009), and the Phonon Liquid Electron Crystal (PLEC) (Liu et al., 2012; Yu et al., 2012) concept. The PLEC concept is an extension of Phonon Glass Electron Crystal and the principle is to eliminate transverse phonon vibrations in the process of heat transfer. The PLEC concept could be successfully applied to copper-based chalcogenides (Ballikaya et al., 2013).

Cu$_{2-x}$Se compound is a known superionic compound that has inherently low thermal conductivity. In the superionic phase, cations exhibit liquid-like diffusivity and the disordered nature results in a low lattice thermal conductivity usually (<1 W/m−K) (Liu et al., 2012; Yu et al., 2012; Ballikaya et al., 2013; Tafti et al., 2016). Cu$_{2-x}$Se based chalcogenides have gained more attention not only because of their extremely low thermal conductivity but also due to their constituent elements (Cu and Se), which are considered benign and are found in abundance in comparison to many other TE material compositions, especially those containing Pb, Sb, As (Tafti et al., 2016). Cu$_{2-x}$Se exists in two phases, a low temperature α phase and a high temperature β phase. The transition from the low temperature to high temperature phase occurs at ~400 K. Se atoms in a Cu$_{2-x}$Se compound are located at FCC sites in the two phases and Cu atoms are coherent and localized in α phase but disordered in β phase (Liu et al., 2012). In spite of Cu-based chalcogenides having promising TE performance, large scale application has been hindered by the reliability issues where diffusive Cu ions are prone to electro-migration; this issue has to be addressed.

Several strategies have been developed to enhance the ZT and the chemical stability of Cu$_{2-x}$Se over a wide temperature range, include tuning of bonding energy (Zhao et al., 2017), developing nanocomposites (Butt et al., 2016; Nunna et al., 2017), chemical doping via transition metals, alkaline, halogen or chalcogenide elements (Peng et al., 2016), and nanoscale incorporation of other elements and compounds (Ballikaya et al., 2019b). Zhao et al. (2017) and Nunna et al. (2017) showed the possibility to obtain ultra-high ZT values in Cu₂Se by incorporating carbon fibers, or carbon nanotubes. Various studies have proved that structural and TE transport properties of Cu$_{2-x}$Se can be modified with a variety of nano-inclusions, and the synthesis route (Tafti et al., 2016; Ballikaya et al., 2019a; Ballikaya et al., 2019b; Hamawandi et al., 2020). Cu$_{2-x}$Se have been synthesized via various methods such as solid-state reaction (Ballikaya et al., 2013), solvo-thermal synthesis (Tafti et al., 2016), melting and annealing (Ballikaya et al., 2019a), high-pressure high-temperature synthesis (Xue et al., 2019), colloidal synthesis (Forster et al., 2017), and arc melting (Butt et al., 2019). In spite of many works reported earlier, the crystal mismatch of guest and host phases on transport properties of Cu$_{2-x}$Se has not been studied in detail. In our previous work, we reported chemical synthesis process and TE properties of nanostructured Cu$_{1.8}$Se and Cu₂Se (Hamawandi et al., 2020). Here, we intend to study the effects of crystal mismatch, using p-type nano-skutterudite inclusion, on the structural and transport properties of nanostructured Cu₂Se.
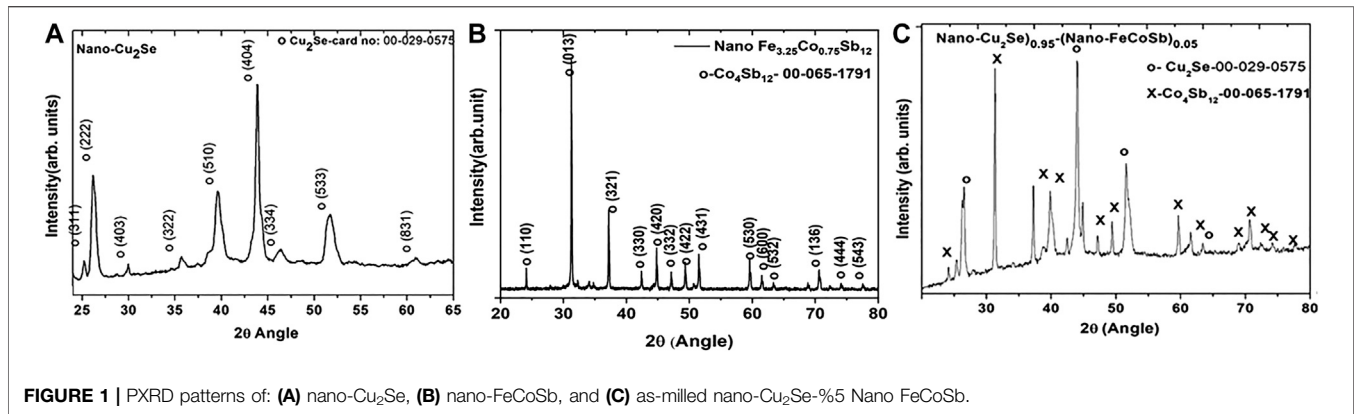
EXPERIMENTAL METHODS

Sample Synthesis
Preparation of Nanoscale Cu$_{2-x}$Se Powders
"Nano Cu$_{2-x}$Se" powders were prepared via a microwave (MW) assisted thermolysis method. High purity copper acetate [Cu(CO$_2$CH$_3$)$_2$·H$_2$O], selenium powder (Se > 99.5) and the organic solvent oleic acid (C$_{18}$H$_{34}$O$_2$), 1-Octadecene (C$_{18}$H$_{36}$, ODE), and trioctylphosphine [P(C$_8$H$_{17}$)$_3$, TOP], methanol and hexane (C$_6$H$_{14}$) were used. The precursor mixture was prepared by adding a stoichiometric amount of copper acetate and Se powder in a MW glass tube with 4 ml of ODE and 8 ml of oleic acid 2 ml of TOP was added in the tube, and then the tube was sealed with silicone septa caps and degassed with several purges of nitrogen followed by vacuum to prevent TOP oxidation. The mixture was stirred for 2 min via MW Synthesizer (Biotage® Initiator) and then heated for 5 min at the synthesis temperature of 250°C using MW power of 400 W. The product was washed several times with methanol and hexane and left in vacuum oven to dry for 3 h at 60°C, thus obtaining dried powder of Cu₂Se. More details on the chemical synthesis process and structural properties of nanostructured Cu₂Se can be found in our previous reports (Tafti et al., 2016; Hamawandi et al., 2020).

Preparation of Nanoscale FeCoSb (Fe$_{3.25}$Co$_{0.75}$Sb$_{12}$) Powders
Precursor for p-type skutterudite nano-FeCoSb powder was prepared by chemical alloying route, using the procedure

FIGURE 1 | PXRD patterns of: **(A)** nano-Cu$_2$Se, **(B)** nano-FeCoSb, and **(C)** as-milled nano-Cu$_2$Se-%5 Nano FeCoSb.

developed and reported earlier (Tafti et al., 2014). The process includes co-precipitation of constituent elements in an intimately mixed oxalate form, which are then thermochemically treated to obtain the final skutterudite phase. In a typical process cobalt chloride (CoCl$_2 \cdot 6H_2O$), iron chloride (FeCl$_2 \cdot 4H_2O$) and antimony chloride (SbCl$_3$) solutions were prepared as stocks. 0.3 M ammonium oxalate (C$_2$H$_8$N$_2$O$_4$) was used as the precipitating agent. Thermodynamic modeling was used to determine the pH window to co-precipitate the constituents with the desired stoichiometry (see Reference Tafti et al., 2014 for further details). The metal ion solution and the precipitating agent were added to the reaction chamber simultaneously. The reaction pH was kept at two and the process was carried out at room temperature. After the precipitation process, the powders were washed, filtered and dried at 60°C overnight. The powders were then calcined at 350°C for 3 h to obtain their oxide form. Finally, to obtain the stoichiometric nano FeCoSb, powders were thermochemically treated at 450°C for 3 h in a rotating tube furnace under hydrogen gas.

Sample Compaction

Cu$_2$Se nanopowders were directly compacted, whereas (nano-Cu$_2$Se)$_{1-x}$(nano-FeCoSb)$_x$ solid solutions were mechanically ground for 1 h in a Planetary Ball Mill (Optosense), then compacted under Argon gas. All powders were loaded into separate 12.6 mm diameter cylindrical dies for compaction using a spark plasma sintering (SPS) system. Then samples were densified at 450°C for 15 min under 50 MPa pressure, cut into disc and rectangular bar shapes for high temperature transport property measurements.

Structural Analysis

The phase identity and purity were verified using powder X-ray diffraction (PXRD) (RigakuUltima IV diffractometer). Scanning electron microscopy (Hitachi S3200 SEM) was used for a detailed microstructural analysis of all the samples.

Transport Properties

Transport property measurements were carried out in the temperature range of 300–800 K. The Seebeck coefficient and electrical conductivity were measured concurrently using Ulvac ZEM-3. The total thermal conductivity κ was calculated according to $\kappa = D.\rho.Cp$, where D is the thermal diffusivity, Cp is the specific heat capacity and ρ is the bulk density. Thermal diffusivity was measured using a LFA1000 laser-based apparatus from Linseis Corporation. Specific heat was measured by a Differential Scanning Calorimeter (Linseis PT1000), and the density obtained from Archimedes' method, reaching about 95–97% of the theoretical density. The typical error bar expected in the Seebeck coefficient and electrical conductivity is ±4%, while it is ±6% for the thermal conductivity.
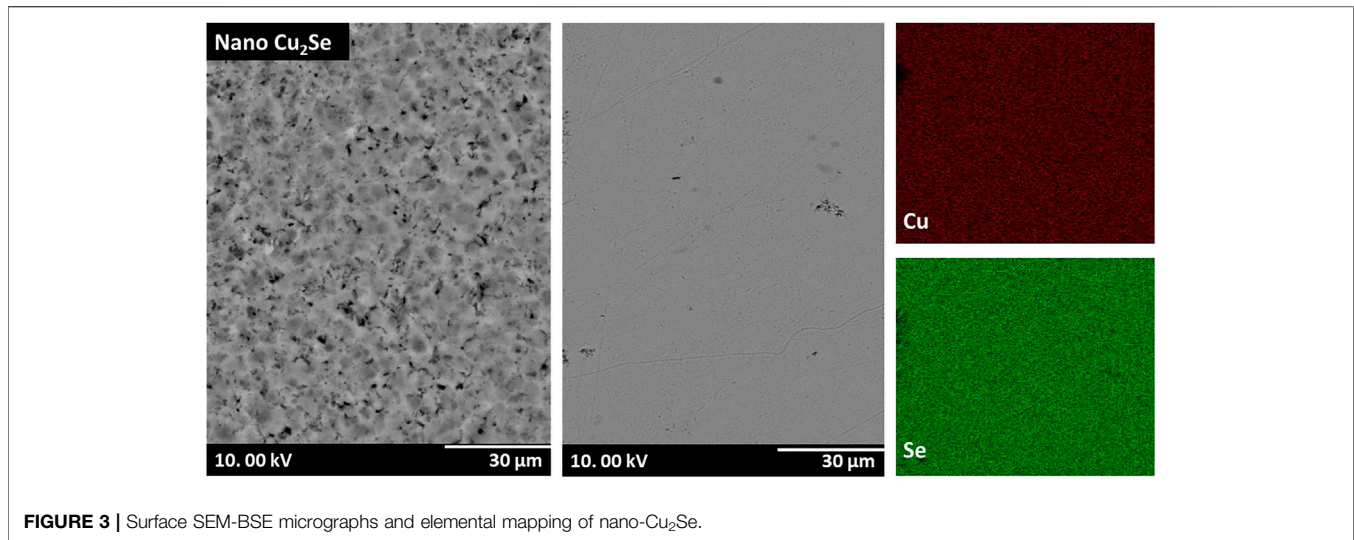
RESULTS AND DISCUSSION

Structural Data

Phase purity of samples were determined by Powder X-Ray Diffraction (PXRD). **Figure 1** shows the PXRD pattern

FIGURE 2 | Fractural nano-Cu$_2$Se SEM micrographs at different magnifications.
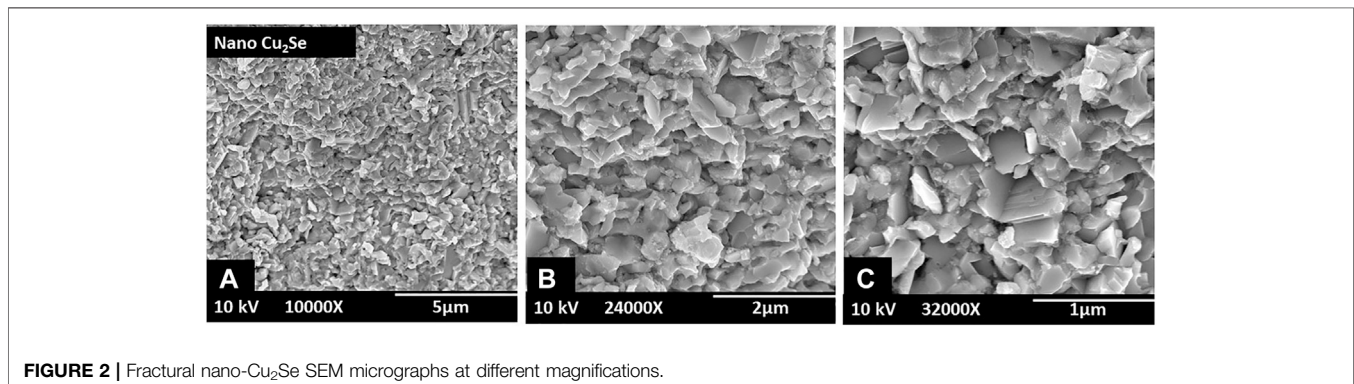
FIGURE 3 | Surface SEM-BSE micrographs and elemental mapping of nano-Cu₂Se.

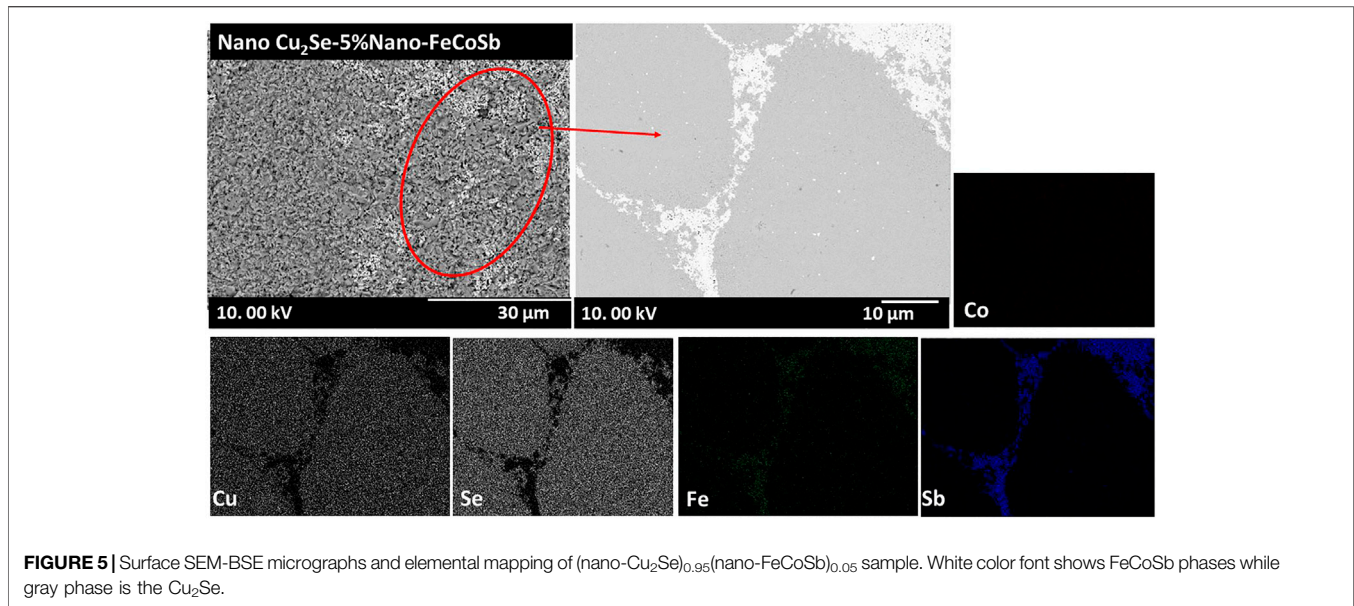obtained from nano-Cu₂Se, nano-FeCoSb, and (Nano-Cu₂Se)₀.₉₅–(Nano-FeCoSb)₀.₀₅.

Figure 1A shows the PXRD pattern of nano-Cu₂Se with orthorhombic crystal structure ((ICDD PDF card no: 00-029–0575)), while the PXRD pattern of nano-FeCoSb ($Fe_{3.25}Co_{0.75}Sb_{12}$),displayed in **Figure 1B**, indicates that all peaks are consistent with the main structure of skutterudite—$CoSb_3$ (ICDD PDF card no: 00-065–1791). The crystal structure of nano-Cu₂Se is rather different from the bulk Cu₂Se (Ballikaya et al., 2013). This is likely because the crystal structure of $Cu_{2-x}Se$ strongly depends on the position and deficiency of Cu atoms in structure (Tafti et al., 2014). **Figure 1C** displays the PXRD pattern of (nano-Cu₂Se)₀.₉₅–(nano-FeCoSb)₀.₀₅, where the presence of two distinct phases, as Cu₂Se and $CoSb_3$ can be clearly observed. This may be a trace of the crystal mismatch between nano-Cu₂Se and nano-FeCoSb. Similar PXRD pattern was obtained for Cu₂Se sample with 2% nano FeCoSb inclusion (data not shown). The diffraction intensity of the minority FeCoSb phase is as strong as the host Cu₂Se phase. The crystal structure of these two phases are different; FeCoSb has a larger unit cell with 32 atoms per cell, where Cu₂Se has 18 atoms

per cell (Uher, 2016). The higher atomic density per unit cell for the skutterudite system may lead to a higher diffraction peak intensity. However, an important contributor to the observed effect could also be the material preparation route, where the FeCoSb skutterudite phase has been reduced by gas-solid reaction at elevated temperature (450°C), therefore exhibiting a higher crystallinity. The crystallinity difference between the Cu₂Se phase and FeCoSb phase can also be seen from the broadening of the diffraction peaks. In the case of Cu₂Se, observed broad diffraction peaks are ascribed to its lower crystallinity as a result of the adapted solution synthesis route.

A more detailed microstructural property evaluation was performed by SEM-EDS analysis. Fractural structure of nano-Cu₂Se is displayed in **Figure 2** at different magnifications. As seen, nano-Cu₂Se has a highly layered texture crystalline structure that is consistent with the literature (Li et al., 2009; Liu et al., 2012; Yu et al., 2012; Ballikaya et al., 2013; Tafti et al., 2016). Its grain size is in the range from 10 nm to 1 μm. In order to further analyze the phase purity element concentration of nano-Cu₂Se, back-scattered electron (BSE) analysis and elemental mapping were performed.
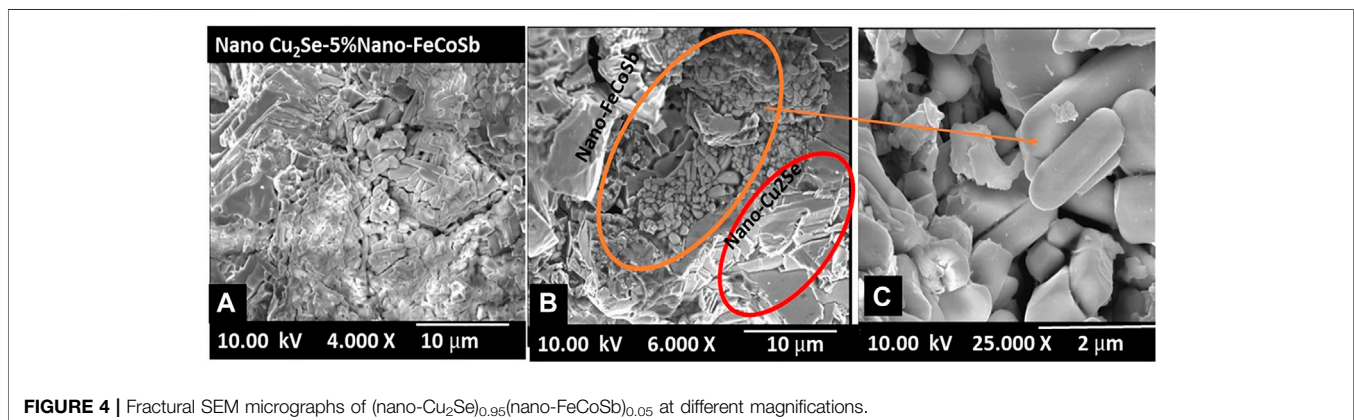
FIGURE 4 | Fractural SEM micrographs of (nano-Cu₂Se)₀.₉₅(nano-FeCoSb)₀.₀₅ at different magnifications.

FIGURE 5 | Surface SEM-BSE micrographs and elemental mapping of $(nano\text{-}Cu_2Se)_{0.95}(nano\text{-}FeCoSb)_{0.05}$ sample. White color font shows FeCoSb phases while gray phase is the Cu_2Se.
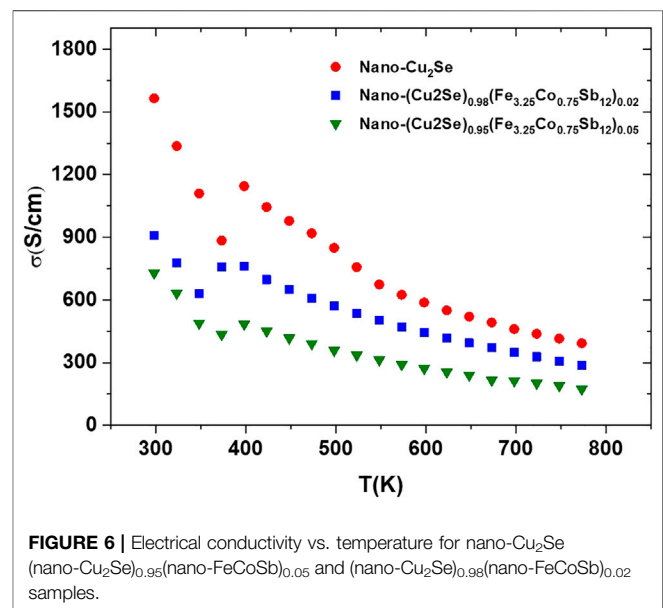
Figure 3 confirms the phase purity of Cu_2Se and homogeny distribution of Cu and Se elements in the structure. **Figure 4** shows SEM micrographs of $(nano\text{-}Cu_2Se)_{0.95}\text{-}(nano\text{-}FeCoSb)_{0.05}$ sample. It clearly reveals that there are two distinct phases as skutterudutie (FeCoSb) and copper chalcogenides (Cu_2Se) in this sample, which is consistent with the PXRD pattern. SEM micrographs of $(nano\text{-}Cu_2Se)_{0.95}\text{-}(nano\text{-}FeCoSb)_{0.05}$ indicates that FeCoSb phase distributed non-uniformly within the structure and form rod shape clusters that are stacked between Cu_2Se layers. Non-uniform distribution of FeCoSb might be due to two possible scenarios. The first one may be the difference in surface energy between FeCoSb and Cu_2Se phases. In other words, small size particles have higher surface energy that resist to combine to form larger grains (Ching and Pan, 2007). Rod shaped FeCoSb nanoparticles might, therefore, resist to combine with larger Cu_2Se particles. The other scenario is the agglomeration of FeCoSb, which may be due to ball milling time and energy not being sufficient for the de-agglomeration of FeCoSb phase for a homogeneous incorporation into the Cu_2Se phase. In order to further investigate the structural properties of Cu_2Se sample with FeCoSb inclusion, a surface SEM-BSE analysis and elemental mapping were performed.
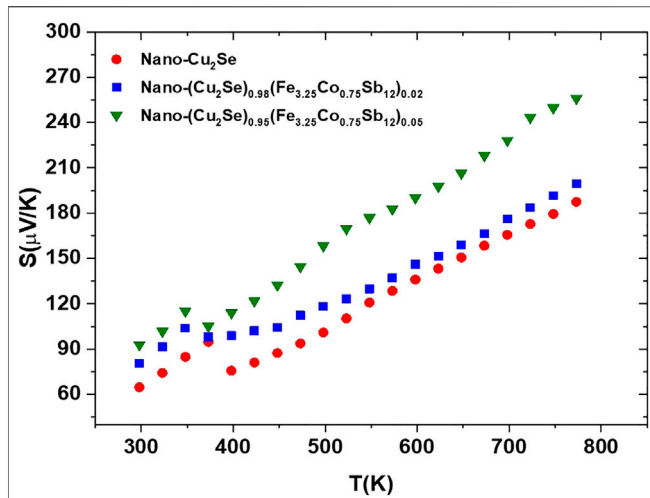
Surface-SEM-BSE micrograph of $(nano\text{-}Cu_2Se)_{0.95}(nano\text{-}FeCoSb)_{0.05}$ in **Figure 5** confirms two different phases as observed from fractural SEM and PXRD patterns. Agglomeration and non-uniform distribution of FeCoSb were clearly observed and it is confirmed with color mapping of the elements. The effect of the observed microstructure of samples on the TE transport properties is presented below.

Transport Properties

All the transport measurements were carried out in the temperature range of 300–800 K. The temperature dependent electrical conductivity is presented in **Figure 6**. Electrical

conductivity decreases with increasing temperature for all samples, which is a typical behavior of highly doped semiconductors. The highest electrical conductivity was obtained in Cu_2Se and the electrical conductivity is suppressed with increasing content of nano-FeCoSb. This may be due to the decrease in charge carrier density with FeCoSb content, or strong scattering of the charge carriers by the grain boundaries. Regarding the second scenario, the decrease in electrical conductivity is thought to be caused by the crystal mismatch between Cu_2Se and FeCoSb phase. As Kim and Majumdar (2006) and Mingo et al. (2009) stated in their work, if there is no homogeneous distribution of nano-phases and there is no coherent interface with small band offsets between the host
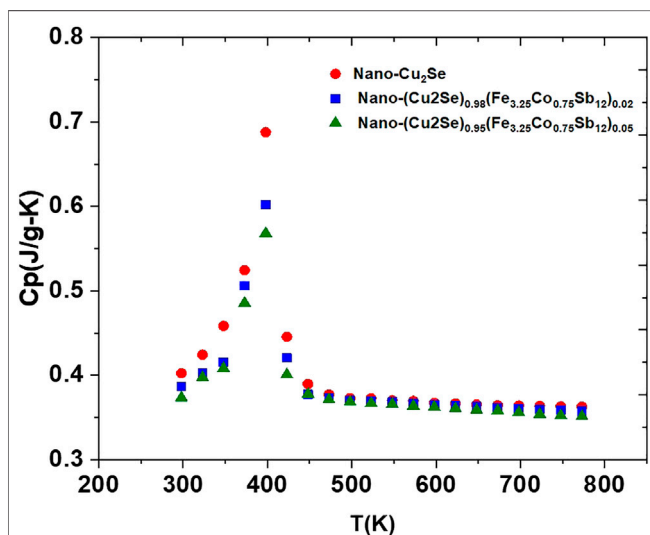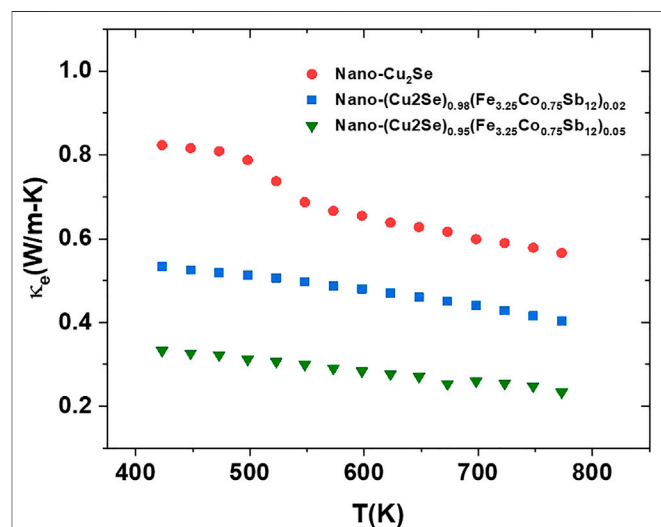

FIGURE 6 | Electrical conductivity vs. temperature for nano-Cu_2Se $(nano\text{-}Cu_2Se)_{0.95}(nano\text{-}FeCoSb)_{0.05}$ and $(nano\text{-}Cu_2Se)_{0.98}(nano\text{-}FeCoSb)_{0.02}$ samples.

FIGURE 7 | Temperature dependent Seebeck coefficient of nano-Cu₂Se (nano-Cu₂Se)₀.₉₅(nano-FeCoSb)₀.₀₅ and (nano-Cu₂Se)₀.₉₈(nano-FeCoSb)₀.₀₂ samples.
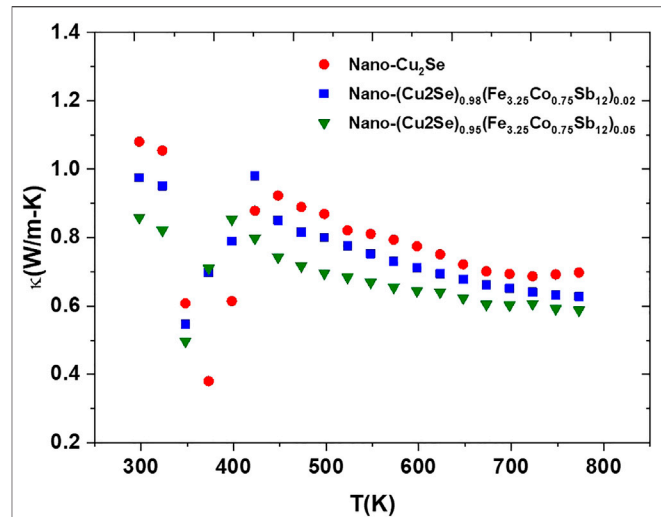
FIGURE 9 | The total thermal conductivity vs. temperature for nano-Cu₂Se (nano-Cu₂Se)₀.₉₅(nano-FeCoSb)₀.₀₅ and (nano-Cu₂Se)₀.₉₈(nano-FeCoSb)₀.₀₂ samples.

FIGURE 8 | The heat capacity, Cp, vs. temperature for nano-Cu₂Se (nano-Cu₂Se)₀.₉₅(nano-FeCoSb)₀.₀₅ and (nano-Cu₂Se)₀.₉₈(nano-FeCoSb)₀.₀₂ samples.

FIGURE 10 | Electronic part of thermal conductivity for nano-Cu₂Se (nano-Cu₂Se)₀.₉₅(nano-FeCoSb)₀.₀₅ and (nano-Cu₂Se)₀.₉₈(nano-FeCoSb)₀.₀₂ samples after the phase transition (400–873 K).

and incorporated nano-phases, then charge carrier scattering is much stronger. Therefore, we believe that crystal mismatch between FeCoSb and Cu₂Se, and agglomeration of FeCoSb phase in the structure might have caused large interfaces to form in the grain boundary regions, which is thought to cause strong scattering of charge carriers.

Positive sign of the Seebeck coefficient in **Figure 7** indicates that holes are the main charge carriers in all samples. The temperature dependent Seebeck coefficient shows generally opposite trend of the temperature dependent electrical conductivity. It seems that the Seebeck coefficient increases with increasing content of FeCoSb,

which is also either due to decreasing charge carrier density, or strong scattering of charge carriers (Uher, 2016; Kim and Majumdar, 2006). The peak observed around 400 K in both the electrical conductivity and the Seebeck coefficient vs. temperature is a signature of well-known structural α-β structural transition in Cu₂Se materials as described earlier (Liu et al., 2012). Heat capacity (C_p) measurement is a useful, indirect method to detect structural changes in a material. All samples reveal a clear signature of a phase transition around 400 K (**Figure 8**). Upon nano FeCoSb inclusion, C_p decreases in comparison to pure nano-Cu₂Se (**Figure 8**). The intensity of a phase transition peak is related to the energy
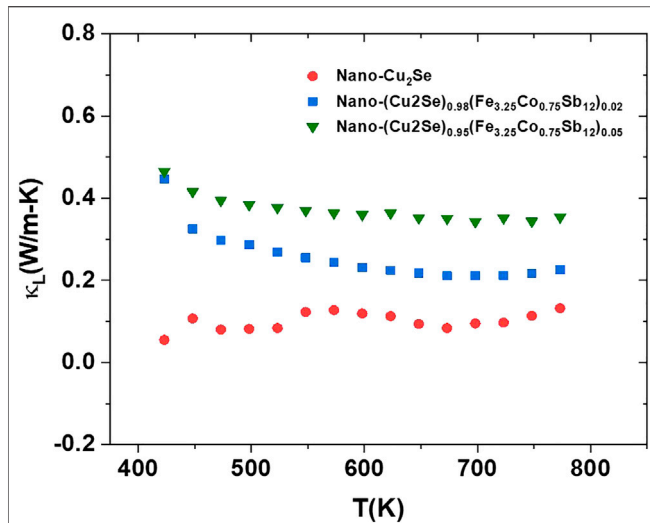
FIGURE 11 | The lattice thermal conductivity, κ_L, vs. temperature for nano-Cu₂Se (nano-Cu₂Se)$_{0.95}$(nano-FeCoSb)$_{0.05}$ and (nano-Cu₂Se)$_{0.98}$(nano-FeCoSb)$_{0.02}$ samples.
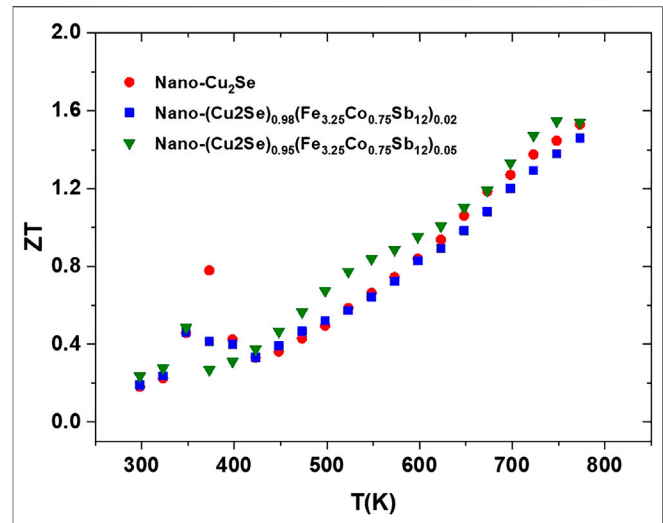
FIGURE 13 | The ZT value of samples as function of temperature for nano-Cu₂Se (nano-Cu₂Se)$_{0.95}$(nano-FeCoSb)$_{0.05}$, and (nano-Cu₂Se)$_{0.98}$(nano-FeCoSb)$_{0.02}$ samples.
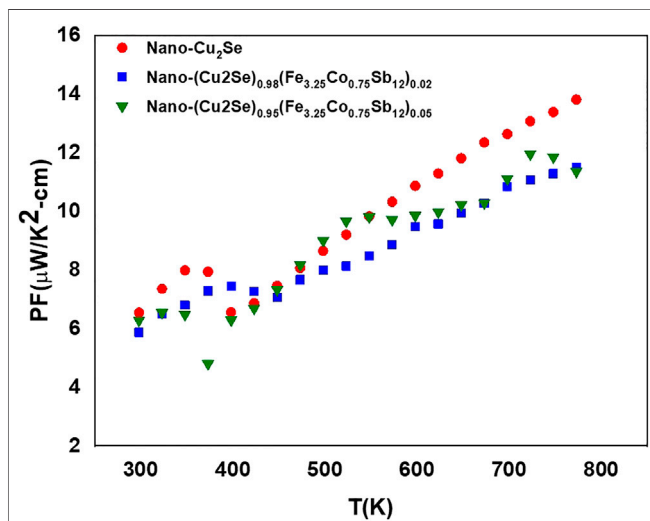
FIGURE 12 | Power factor (PF) function of temperature for nano-Cu₂Se (nano-Cu₂Se)$_{0.95}$(nano-FeCoSb)$_{0.05}$ and (nano-Cu₂Se)$_{0.98}$(nano-FeCoSb)$_{0.02}$ samples.

difference between the two phases, and it also reflects the chemical stability of compound (Brown, 2015; Ballikaya et al., 2019b). In other words, compounds that have small peak during phase transition are more stable thermally and chemically in comparison to those with a higher peak intensity. Therefore, it may be concluded that the thermal stability of these samples also increases with increasing nano FeCoSb content (Brown, 2015; Olvera et al., 2017).

The total thermal conductivity for all the samples as a function of temperature is shown in **Figure 9**. The thermal conductivity is

suppressed with increasing nano-FeCoSb content. In order to further understand this issue, the electronic and lattice part of the thermal conductivity were evaluated separately. Wiedemann-Franz law was used to calculate the lattice contribution to the thermal conductivity (κ_L) of all the samples by deducting the electronic term ($\kappa_e = L\sigma T$, where L, σ and T are the Lorenz number, electrical conductivity and absolute temperature, respectively) from the total thermal conductivity. The values of L for all the compounds were calculated by using the following equations (Ballikaya et al., 2013):

$$L = \left[\frac{k_B}{e}\right]^2 \left[\frac{(r + 7/2)F_{r+5/2}(\xi)}{(r + 3/2)F_{r+1/2}(\xi)} - \left[\frac{(r + 5/2)F_{r+3/2}(\xi)}{(r + 3/2)F_{r+1/2}(\xi)}\right]^2\right] \quad (1)$$

where r is the charge carrier scattering parameter, k_B the Boltzmann constant, e the electron charge, and $F_n(\xi)$ is the Fermi integral given by

$$F_n(\xi) = \int_0^\infty \frac{\chi^n}{1 + e^{\chi - \xi}} d\chi, \quad (2)$$

Here, ξ is the reduced Fermi energy that can be calculated from the Seebeck coefficient, S and the scattering parameter r according to

$$S = \pm \frac{k_B}{e} \frac{(r + 5/2)F_{r+3/2}(\xi)}{(r + 3/2)F_{r+1/2}(\xi)} - \xi \quad (3)$$

It is assumed that the system is highly degenerate, and scattering was dominated by acoustic phonons. The temperature dependent Lorenz number is estimated as 2.21 to 1.55×10^{-8} V²/K² in the temperature range of 300–800 K for the analyzed samples. Temperature dependent κ_e values in the temperature range of 300–800 K are shown in **Figure 10**.

As clearly seen, the highest κ_e values belong to Cu$_2$Se, which is due to its higher electrical conductivity. The κ_e decreases with increasing content of FeCoSb phase. This is also associated with decrease in the electrical conductivity. When electronic conductivity value of samples at 400 and 873 K are compared, it can be seen that the gap between maximum and minimum values is 40, 30, and 50% for pure nano Cu$_2$Se samples, and samples with 2 and 5% FeCoSb inclusion, respectively. This indicates that the electronic thermal conductivity plays a rather effective role in the reduction of thermal conductivity of nano-Cu$_2$Se, and samples with 2 and 5% FeCoSb inclusion. The temperature dependent lattice thermal conductivities of samples are shown in **Figure 11**.

A minimum lattice thermal conductivity value of 0.19 W/mK was obtained in nano-Cu$_2$Se. This might be because this sample has a highly textured structure, consisting of a large number of smaller grains (Hicks and Dresselhaus, 1993; Hori and Shiomi, 2019). As it is known, there are three different phonon modes that contribute to the thermal conductivity in solids which are low, medium, and high frequency. Among these, low frequency phonons have higher contribution in lattice thermal conductivity due to their larger mean free path (Hicks and Dresselhaus, 1993; Hori and Shiomi, 2019). Micro-nano size grain is responsible for low and medium frequency phonon scattering. This might be the dominant reason for observing lower lattice thermal conductivity in nano-Cu$_2$Se.

The power factor (PF) is calculated using electrical conductivity combined with the Seebeck coefficient. The PF vs. temperature plot for all the samples is given in **Figure 12**. The maximum power factor of 14 μW/(mK^2) at 800 K was achieved for Cu$_2$Se sample, due to its higher electrical conductivity and relatively high Seebeck coefficient.

The temperature dependent figure of merit for all samples are presented in **Figure 13**. The ZT values of all samples are higher than some of the reported ZT values for bulk and nanostructured Cu$_{2-x}$Se samples over 900 K (Liu et al., 2012; Yu et al., 2012; Ballikaya et al., 2013; Oztan et al., 2020). The maximum ZT value reached ~1.6 at 750 K for the (nano-Cu$_2$Se)$_{0.95}$(nano-FeCoSb)$_{0.05}$ sample which is one of the highest ZT values for Cu$_2$Se reported at this temperature. This indicates that it is possible to further enhance the ZT value with optimization of nano-FeCoSb content and its distribution within the nano-Cu$_2$Se phase.

CONCLUSION

Nano-Cu$_2$Se and p-type skutterudite Fe$_{3.25}$Co$_{0.75}$Sb$_{12}$ compounds were synthesized successfully by using microwave assisted thermolysis and chemical alloying route, respectively. Their solid solutions (Cu$_2$Se with 2 and 5% nano-FeCoSb) were prepared via mechanical alloying followed by SPS process.

Detailed structural analyses of all samples were performed by SEM-EDS, PXRD, and transport properties were evaluated via Seebeck coefficient, electrical conductivity and thermal conductivity measurements. SEM-EDS pattern with PXRD analysis of samples shows Cu$_2$Se and Fe$_{3.25}$Co$_{0.75}$Sb$_{12}$ have a single phase while the FeCoSb included sample consists of two phases from FeCoSb and Cu$_2$Se. The micro-structure of the (Nano-Cu$_2$Se)$_{1-x}$(Nano FeCoSb)$_x$ sample showed that rod shape nano FeCoSb was distributed non-uniformly and formed clusters that stacked between Cu$_2$Se layers. Transport data indicated that electrical conductivity decreased with inclusion of nano-FeCoSb. This is attributed to strong scattering of charge carriers on grain boundaries originated from crystal mismatch between Cu$_2$Se and FeCoSb. Thermal conductivity evaluation shows electronic thermal conductivity plays a major role in the reduction of thermal conductivity with FeCoSb inclusions. The maximum ZT value reached ~1.6 at 750 K with %5 FeCoSb inclusion, which is ~%15 higher than nano-Cu$_2$Se (ZT~1.4 at 750 K) at this temperature. This is one of the highest ZT values reported for Cu$_{2-x}$Se at this temperature. Structural and transport data show that nano FeCoSb incorporation in Cu$_2$Se has a beneficial effect on the TE performance up to 800 K, and it may be possible to further enhance it with the optimization of concentration and distribution of nano-FeCoSb phase within Cu$_2$Se.

DATA AVAILABILITY STATEMENT

The original contributions presented in the study are included in the article/Supplementary Material, further inquiries can be directed to the corresponding authors.

AUTHOR CONTRIBUTIONS

YD, AY, and SB drafted the manuscript; SB, BH, and MT conceptualized; YD, AY, and BH conducted the experiment, SB and MT reviewed the manuscript.

FUNDING

REFERENCES

Ballikaya, S., Chi, H., Salvador, J. R., and Uher, C. (2013). Thermoelectric properties of Ag-doped Cu$_2$Se and Cu$_2$Te. *J. Mater. Chem.* 1, 12478–12484. doi:10.1039/c3ta12508d

Ballikaya, S., Oner, Y., Temel, T., Ozkal, B., Bailey, T. P., Toprak, M. S., et al. (2019a). Thermoelectric and thermal stability improvements in Nano-Cu$_2$ Se included Ag$_2$ Se. *J. Solid State Chem.* 273, 122–127. doi:10.22226/2410-3535-2013-2-87-90

Ballikaya, S., Sertkol, M., Oner, Y., Bailey, T. P., and Uher, C. (2019b). Fracture structure and thermoelectric enhancement of Cu$_2$Se with substitution of

nanostructured Ag₂Se. *Phys. Chem. Chem. Phys.* 21 (25), 13569–13577. doi:10. 2991/iceesd-18.2018.319

Beekman, M., Morelli, D., and Nolas, G. (2015). Better thermoelectrics through glass-like crystals. *Nat. Mater.* 14, 1182–1185. doi:10.1088/1674-1056/abbbf5

Bell, L. E. (2008). Cooling, heating, generating power, and recovering waste heat with thermoelectric systems. *Science* 321 (5895), 1457–1461. doi:10.1134/1.1513855

Brown, D. (2015). *Enhanced thermoelectric performance at the superionic phase transitions of mixed ion-electron conducting materials.* Dissertation (Ph.D.) California Institute of Technology. doi:10.7907/Z9B56GNM

Butt, S., Farooq, M. U., Mahmood, W., Salam, S., Sultan, M., Basit, M. A., et al. (2019). One-step rapid synthesis of Cu₂Se with enhanced thermoelectric properties. *J. Alloys Compd.* 786, 557–564. doi:10.1002/chin.199817023

Butt, S., Xu, W., Farooq, M. U., Ren, G. K., Zhang, Q., Zhu, Y., et al. (2016). Enhanced thermoelectricity in high-temperature β-phase copper (I) selenides embedded with Cu₂Te nanoclusters. *ACS Appl. Mater. Interfaces* 8 (24), 15196–15204.

Ching, H. N., and Pan, J. (2007). Sintering of particles of different sizes. *Acta Mater.* 55, 813–824. doi:10.1557/proc-1166-n03-26

Forster, J. D., Lynch, J. J., Coates, N. E., Liu, J., Jang, H., Zaia, E., et al. (2017). Solution processed Cu₂Se nanocrystal films with bulk like thermoelectric performance. *Sci. Rep.* 7 (1), 1–7. doi:10.1021/acsami.9b01718.s001

Hamawandi, B., Ballikaya, S., Rasander, M., Halim, J., Vinciguerra, L., Rosen, J., et al. (2020). Composition tuning of nanostructured binary copper selenides through rapid chemical synthesis and their thermoelectric property evaluation. *Nanomaterials* 10, 854. doi:10.1021/acsaem.0c01525.s001

Heremans, J. P., Jovovic, V., Toberer, E. S., Saramat, A., Kurosaki, K., Charoenphakdee, A., et al. (2008). Enhancement of thermoelectric efficiency in PbTe by distortion of the electronic density of state. *Science.* 321(5888), 554–557. doi:10.1021/acsaem.9b01016.s001

Hicks, L. D., and Dresselhaus, M. S. (1993). Effect of quantum-well structures on the thermoelectric figure of merit. *Phys. Rev. B.* 47 (19), 12727. doi:10.1109/ict. 1996.553525

Hori, T., and Shiomi, J. (2019). Tuning phonon transport spectrum for better thermoelectric materials. *Sci. Technol. Adv. Mater.* 20 (1), 10–25. doi:10.1557/ proc-281-821

Hsu, K. F., Loo, S., Goo, F., Chen, W., Dyck, J. S., Uher, C., et al. (2004). Cubic AgPbmSb: bulk thermoelectric materials with high figure of merit. *Science* 303 (5659), 818–821. doi:10.1557/proc-452-261

Julian Goldsmid, H. (2009). *Introduction to thermoelectricity.* Berlin: Springer-Verlag.

Kim, W., and Majumdar, A. (2006). Phonon scattering cross section of polydispersed spherical nanoparticles. *J. Appl. Phys.* 99 (8), 084306. doi:10. 1103/physrevb.47.12727

Li, H., Tang, X., Zhang, Q., and Uher, C. (2009). High performance In$_x$Ce$_y$Co$_4$Sb$_{12}$ thermoelectric materials with *in situ* forming nanostructured InSb phase. *Appl. Phys. Lett.* 94 (10), 102114. doi:10.1134/1.1500470

Liu, H., Shi, X., Xu, F., Zhang, L., Zhang, W., Chen, L., et al. (2012). Copper ion liquid-like thermoelectrics. *Nat. Mater.* 11 (5), 422–425. doi:10.1109/ict.1997.667182

Liu, W., Tan, X., Yin, K., Liu, H., Tang, X., Shi, J., et al. (2012). Convergence of conduction bands as a means of enhancing thermoelectric performance of n-type Mg₂Si$_{1-x}$Sn$_x$ solid solutions. *Phys. Rev. Lett.* 108 (16), 166601. doi:10. 1557/proc-545-369

Mingo, N., Hauser, D., Kobayashi, N. P., Plissonnier, M., and Shakouri, A. (2009). Nanoparticle-in-Alloy approach to efficient thermoelectrics: silicides in SiGe. *Nano Lett.* 9 (2), 711–715. doi:10.1109/ict.1999.843472

Morelli, D. T., Jovovic, V., and Heremans, J. P. (2008). Intrinsically minimal thermal conductivity in cubic I–V–VI₂ semiconductors. *Phys. Rev. Lett.* 101 (3), 035901. doi:10.1103/physrevb.53.r10493

Nunna, R., Qiu, P., Yin, M., Chen, H., Hanus, R., Song, Q., et al. (2017). Ultrahigh thermoelectric performance in Cu₂Se-based hybrid materials with highly dispersed molecular CNTs. *Enery. Environ. Sci.* 10 (9), 1928–1935. doi:10. 1039/c7ee01737e

Olvera, A., A Moroz, N., Sahoo, P., Ren, P., P Bailey, T., Page, A., et al. (2017). Partial indium solubility induces chemical stability and colossal thermoelectric figure of merit in Cu₂Se. *Energy Environ. Sci.* 10 (7), 1668–1678. doi:10.1021/ acsami.9b01718.s001

Oztan, C. Y., Hamawandi, B., Zhou, Y., Ballikaya, S., Toprak, M. S., Leblanc, R., et al. (2020). Thermoelectric performance of Cu₂Se doped with rapidly synthesized gel-like carbon dots. *J. Alloys Compd.* 13, 157916. doi:10.1016/j. jallcom.2020.157916

Pei, Y., Shi, X., LaLonde, A., Wang, H., Chen, L. D., and Snyder, G. J. (2011). Convergence of Electronic bands for high performance bulk thermoelectrics. *Nature* 473 (7345), 66–69. doi:10.1021/acsaem.0c01525.s001

Peng, P., Gong, Z. N., Liu*, F. S., Huang, M. J., Ao, W. Q., Li, Y., et al. (2016). Structure and thermoelectric performance of β-Cu₂Se doped with Fe, Ni, Mn, In, Zn or Sm. *Intermetallics* 75, 72–78. doi:10.1021/acsami.9b08699.s001

Poudel, B., Hao, Q., Ma, Y., Lan, Y., Minnich, A., Yu, B., et al. (2008). High thermoelectric performance of nanostructured bismuth antimony telluride bulk alloys. *Science.* 320 (5876), 634–638. doi:10.1007/978-981-13-2889-3_20

Rowe, D. M. Editor (2006). *Thermoelectrics handbook: macro to nano.* Boca Raton: CRC/Taylor & Francis.

Snyder, G. J., Toberer, E. S., and Snyder, G. J. (2008). Complex thermoelectric materials. *Nat. Mater.* 7, 105–114. doi:10.1016/j.matlet.2019.05.009

Tafti, M. Y., Ballikaya, S., Khachatourian, A. M., Noroozi, M., Saleemi, M., Han, L., et al. (2016). Promising bulk nanostructured Cu2Se thermoelectrics: via high throughput and rapid chemical synthesis. *RSC Adv.* 6, 111457–111464. doi:10. 2991/iceesd-18.2018.319

Tafti, M. Y., Saleemi, M., Toprak, M. S., Johnsson, M., Jacquot, A., Jagle, M., et al. (2014). Fabrication and characterization of nanostructured thermoelectric Fe$_x$Co$_{1-x}$Sb₃. *Open Chem.* 1, 629. doi:10.1021/acsaem.9b01537.s001

Uher, C. (2016). *Material aspect of thermoelectricity.* Boca Raton, FL: CRC Press, Taylor and Francis.

Xue, L., Zhang, Z., Shen, W., Ma, H., Zhang, Y., Fang, C., et al. (2019). Thermoelectric performance of Cu₂Se bulk materials by high-temperature and high-pressure synthesis. *J. Mater.* 5 (1), 103–110. doi:10.2172/1223723

Yu, B., Liu, W., Chen, S., Wang, H., Wang, H., Chen, G., et al. (2012). Thermoelectric properties of copper selenide with ordered selenium layer and disordered copper layer. *Nanomater. Energy* 1 (3), 472–478. doi:10. 2172/1561264

Zhao, K., Blichfeld, A. B., Chen, H., Song, Q., Zhang, T., Zhu, C., et al. (2017). Enhanced thermoelectric performance through tuning bonding energy in Cu₂Se$_{1-x}$S$_x$ liquid-like materials. *Chem. Mater.* 29 (15), 6367–6377. doi:10. 5772/intechopen.72453

Conflict of Interest: The authors declare that the research was conducted in the absence of any commercial or financial relationships that could be construed as a potential conflict of interest.